# How big is the influence of biogenic silicon pools on short-term changes of water soluble silicon in soils? Implications from a study of a ten-year-old plant-soil-system

**Daniel Puppe[a,*], Axel Höhn[a], Danuta Kaczorek[b], Manfred Wanner[c], Marc Wehrhan[a], Michael Sommer[a,d]**

[a] Leibniz-Centre for Agricultural Landscape Research (ZALF) e.V., Institute of Soil Landscape Research, 15374 Müncheberg, Germany

[b] Department of Soil Environment Sciences, Warsaw University of Life Science (SGGW), Nowoursynowska 159, 02-776 Warsaw, Poland

[c] Brandenburg University of Technology Cottbus-Senftenberg, Department Ecology, 03013 Cottbus, Germany

[d] University of Potsdam, Institute of Earth and Environmental Sciences, 14476 Potsdam, Germany

* Corresponding author. E-mail address: daniel.puppe@zalf.de

**Abstract**

The significance of biogenic silicon (BSi) pools as a key factor for the control of Si fluxes from terrestrial to aquatic ecosystems has been recognized since decades. However, while most research has been focused on phytogenic Si pools, knowledge on other BSi pools is still limited. We hypothesized different BSi pools to influence short-term changes of the water soluble Si fraction in soils to different extents. To test our hypothesis we took plant (*Calamagrostis epigejos*, *Phragmites australis*) and soil samples in an artificial catchment in a post-mining landscape in the state of Brandenburg, Germany. We quantified phytogenic

(phytoliths), protistic (diatom frustules and testate amoeba shells) and zoogenic (sponge spicules) Si pools as well as Tiron extractable and water soluble Si fractions in soils at the beginning ($t_0$) and after ten years ($t_{10}$) of ecosystem development. As expected the results of Tiron extraction showed, that there are no consistent changes of the amorphous Si pool at 'Chicken Creek' as early as after ten years. In contrast, compared to $t_0$ we found increased water soluble Si and BSi pools at $t_{10}$, thus we concluded BSi pools to be the main driver of short-term changes of water soluble Si. However, because total BSi represents only small proportions of water soluble Si at $t_0$ (<2 %) and $t_{10}$ (2.8-4.3 %) we further concluded smaller (<5 µm) and/or fragile phytogenic Si structures to have the biggest impact on short-term changes of water soluble Si. In this context, extracted phytoliths (>5 µm) only amounted to about 16 % of total Si contents of plant materials of *C. epigejos* and *P. australis* at $t_{10}$, thus about 84 % of small-scale and/or fragile phytogenic Si are not quantified by the used phytolith extraction method. Analyses of small-scale and fragile phytogenic Si structures are urgently needed in future work as they seem to represent the biggest and most reactive Si pool in soils, thus the most important driver of Si cycling in terrestrial biogeosystems.

**Keywords**

biosilicification, initial biogeosystem, phytogenic Si, protistic Si, zoogenic Si

## 1. Introduction

Various prokaryotes and eukaryotes are able to synthesize hydrated amorphous silica ($SiO_2 \cdot nH_2O$) structures from monomeric silicic acid ($H_4SiO_4$), a process called biosilicification (Ehrlich et al. 2010). In terrestrial biogeosystems biogenic silicon (BSi) synthesized by bacteria and fungi, plants, diatoms, testate amoebae and sponges can be found forming corresponding microbial, phytogenic, protophytic, protozoic and zoogenic BSi pools, respectively (Puppe et al. 2015, Sommer et al. 2006). BSi has been recognized as a key factor for the control of Si fluxes from terrestrial to aquatic ecosystems as it is in general more soluble compared to silicate minerals (e.g., Fraysse et al. 2006, 2009). These fluxes influence marine diatom production on a global scale (Dürr et al. 2011, Sommer et al. 2006, Struyf & Conley 2012). Marine diatoms in turn can fix large quantities of carbon dioxide via photosynthesis because up to 54 % of the biomass in the oceans is represented by diatoms, thus diatoms have an important influence on climate change (Tréguer & De La Rocha 2013, Tréguer & Pondaven 2000).

While the importance of phytogenic Si pools for global Si fluxes has been recognized for three decades (e.g., Bartoli 1983, Meunier et al. 1999, Street-Perrott & Barker 2008), information on the other BSi pools is comparably rare (Clarke 2003). However, in recent publications the potential importance of diatoms, testate amoebae and sponge spicules in soils for Si cycling has been highlighted (Aoki et al. 2007, Creevy et al. 2016, Puppe et al. 2014, 2015, 2016). Furthermore, evidence arises that BSi pools are in disequilibrium at decadal time scales due to disturbances and perturbations by humans, e.g., by changes in forest management or farming practices (Barão et al. 2014, Keller et al. 2012, Vandevenne et al. 2015). In consequence, BSi accumulation and BSi dissolution are not balanced, which influences Si cycling in terrestrial biogeosystems not only on decadal but also on millennial

scales (Clymans et al. 2011, Frings et al. 2014, Sommer et al. 2013, Struyf et al. 2010). Sommer et al. (2013), for example, found the successive dissolving of a relict phytogenic Si pool to be the main source of dissolved Si in soils of a forested biogeosystem. Due to the fact that the continuous decomposition of this relict phytogenic Si pool is not compensated by an equivalent buildup by recent vegetation the authors concluded a BSi disequilibrium on a decadal scale. On a millennial scale Clymans et al. (2011) estimated the total amorphous Si storage in temperate soils to be decreased by approximately 10 % since the onset of agricultural development about 5,000 years ago. This decrease not only has consequences for land-ocean Si fluxes but also influences agricultural used landscapes because Si is a beneficial element for many crops (e.g., Epstein 2009, Ma & Yamaji 2008).

For a better understanding of BSi dynamics, chronosequence studies are well suited, because they allow us to analyze time-related changes of BSi pools during biogeosystem development. In the present study we analyzed various BSi pools in differently aged soils of an initial artificial catchment ('Chicken Creek') in a post-mining landscape in NE Germany. Chicken Creek represents a study site with defined initial conditions and offers the rare opportunity to monitor BSi dynamics from the very beginning. Former studies at this site revealed i) a formation of protophytic (diatom frustules), protozoic (testate amoeba shells) and zoogenic (sponge spicules) Si pools within a short time (<10 years) and ii) a strong relation of spatiotemporal changes of protistic (diatoms and testate amoebae) BSi pools to the vegetation, because plants provide, e.g., rhizospheric micro-habitats including enhanced food supply (Puppe et al. 2014, 2016). From these results it can be concluded that especially vegetated spots at initial biogeosystem sites represent hot spots of BSi accumulation of various origin (compare Wanner & Elmer 2009). Furthermore, construction work with large machines resulted in differently structured sections of Chicken Creek with slight differences

97 in abiotic conditions (for details see subsection 2.1.) (Gerwin et al. 2010). These differences
98 in turn lead to section-specific vegetation dynamics at Chicken Creek (Zaplata et al. 2010).
99 Knowledge about BSi accumulation dynamics is crucial for the understanding of Si cycling in
100 terrestrial biogeosystems. We regard water extractable Si as an useful proxy for desilication
101 and biological uptake (plants, testate amoebae etc.). In addition, we used an alkaline
102 extractant (Tiron) to detect eventual short-term changes of the amorphous Si fraction. We
103 hypothesized i) BSi pools to influence short-term changes of water soluble Si in initial soils,
104 but no short-term changes in amorphous Si fractions, ii) the phytogenic Si pool to be the
105 most prominent one in size, thus the biggest driver of short-term changes of water soluble
106 Si, and iii) BSi pool changes to be section-specific, i.e., related to vegetation dynamics. The
107 aims of the present study were i) to quantify various BSi pools, i.e., protophytic, protozoic,
108 zoogenic and phytogenic Si pools, during initial soil and ecosystem development, (ii) to
109 analyze potential section-specific short-term changes of these BSi pools after a decade of
110 ecosystem development, and iii) to evaluate the influence of different BSi pools on water
111 soluble Si in these soils.
112
113 **2. Material and methods**
114 *2.1. Study site*
115 The study site Chicken Creek (51°36'18" N, 14°15'58" E) represents an artificial catchment in
116 a post-mining landscape located in the active mining area 'Welzow-South' (lignite open-cast
117 mining, 150 km south-east of Berlin) in the state of Brandenburg, Germany (Kendzia et al.
118 2008, Russell et al. 2010). Climate at Chicken Creek is characterized by an average air
119 temperature of 9.6°C and an annual precipitation of 568 mm comprising data from 1981 to
120 2010 (Meteorological Station Cottbus, German Weather Service).

For construction of the about 6 ha sized catchment an 1-3 m thick base layer (aquiclude) of Tertiary clay was covered by a 2-3 m thick sandy, lignite- and pyrite-free Quaternary sediment serving as water storage layer (aquifer) (Gerwin et al. 2010, Kendzia et al. 2008). Quaternary material was taken from a depth of 20-30 m during lignite mining process and its texture is classified as sand to loamy sand (Table 1) with low contents of carbonate (Gerwin et al. 2009, 2010, Russell et al. 2010). Dumping of material and construction work with large machines (e.g., stackers and bulldozers) resulted in differently structured sections of Chicken Creek. Generally, the catchment area can be divided into four sections: i) an eastern part (ca. 1.8 ha), ii) a western part (ca. 1.6 ha), iii) a central trench (ca. 0.9 ha) separating the eastern from the western part and iv) a southern part (ca. 1.5 ha) with a pond at the lowest point (Fig. 1). Construction work was completed in September 2005 (time zero, $t_0$). Analyses subsequent to catchment completion indicated slight differences in abiotic conditions (soil pH, conductivity, skeleton content (soil particle diameter >2 mm), proportions of sand, silt and clay, concentration of organic and inorganic carbon) between the eastern and the western part (Gerwin et al. 2010). The primary mineral component in all particle size fractions at $t_0$ was quartz (only small amounts of K-feldspar, plagioclase). Calcite comprised 0.5-4.5 % of the initial sediment, dolomite was only detectable in few samples with contents of 0.5 % and magnesite ($MgCO_3$) was not detectable by mineralogical analysis (W. Schaaf, pers. comm., 2011). For detailed information on site construction and initial ecosystem development see Gerwin et al. (2010) and Schaaf et al. (2010), respectively.

*2.2. Soil sampling*

We took samples shortly after construction of Chicken Creek (2005, $t_0$) and after an ecosystem development period of about ten years (2015, $t_{10}$). For $t_0$ (no vegetation

detectable) we assumed only very few biogenic siliceous structures homogenously distributed on the whole area of Chicken Creek, i.e., no section-specific distribution of BSi (BSi $t_0$ east ≈ BSi $t_0$ west ≈ BSi $t_0$ south) at the beginning of ecosystem development (Puppe et al. 2016). This is why we did not sample all different sections of the catchment, but took soil samples in six field replicates to quantify BSi pools at $t_0$. However, for $t_{10}$ we hypothesized section-specific differences in BSi pool quantities related to section-specific vegetation dynamics. To evaluate these differences after a decade of ecosystem development and to cover the biggest possible BSi accumulation in soil we focused on spots where Si accumulating plant species, i.e., *Calamagrostis epigejos* and *Phragmites australis* became dominant (Zaplata et al. 2010). Thus we took samples in the eastern (*C. epigejos* dominant) and western (mainly *C. epigejos* dominant, one spot with *P. australis*) and southern section (*P. australis* dominant) of Chicken Creek.

For an accurate description of changes of abiotic soil conditions and related phytogenic Si in every section we took soil and plant samples in eastern, western and southern sections at $t_0$ as well as $t_{10}$. Erosion and deposition processes were clearly evident in the Chicken Creek catchment during the first years without plant cover. Substantial surface changes resulted from rill erosion as aerial photographs (rill network) and a comparison of photogrammetry-based digital elevation models showed (Schneider et al. 2013). Interrill erosion did not lead to surface changes larger than about 20 cm during the first five years. Afterwards the establishment of an area-wide plant cover substantially reduces interrill erosion. Because all soil data at $t_0$ referred to a depth increment of 30 cm we reasonably assumed the same soil conditions for the sampled $t_0$-spots during the first years. Furthermore, we carefully selected sampling points at $t_{10}$ to be not influenced by erosion, i.e., at spots with low surface roughness and outside rills. Soil samples for the determination of soil properties and plant

169 samples were taken in five (western and southern section) and six (eastern section) field
170 replicates at $t_0$ and $t_{10}$ (Fig. 1). At every sampling point three undisturbed soil cores where
171 taken with a core cutter (diameter = 3.4 cm, depth = 5 cm) and transferred into plastic bags.
172 Bulk densities were calculated from dividing weight of dried (105°C) soil samples by
173 corresponding volume.
174
175 *2.3. Determination of basic soil properties*
176 Soil samples were air dried and sieved and the fine earth fraction (<2 mm) was used for
177 laboratory analyses. Soil pH was measured based on the DIN ISO Method 10390 (1997) in
178 0.01 M $CaCl_2$ suspensions at a soil to solution ratio of 1:5 (*w/v*) after a 60 minute
179 equilibration period using a glass electrode. The total carbon content was analyzed by dry
180 combustion using an elemental analyzer (Vario EL, Elementar Analysensysteme, Hanau,
181 Germany). Carbonate ($CaCO_3$) was determined conductometrically using the Scheibler
182 apparatus (Schlichting et al. 1995). Organic carbon ($C_{org}$) was computed as the difference
183 between total carbon and carbonate carbon. Analyses of basic soil properties were
184 performed in two lab replicates per sample.
185
186 *2.3.1. Water Extractable Si ($Si_{H2O}$)*
187 Water extractable Si was determined based on a method developed by Schachtschabel &
188 Heinemann (1967). Ten grams of dry soil (<2 mm) were weighed into 80 mL centrifuge tubes
189 and 50 mL distilled water added together with three drops of a 0.1% $NaN_3$-solution to
190 prevent microbial activity. Total extraction time was seven days in which tubes were shaken
191 by hand twice a day for twenty seconds. Mechanical (constant) shaking by using, e.g., a roll
192 mixer, was avoided to prevent abrasion of mineral particles colliding during shaking

193 (McKeague & Cline 1963). The solutions were centrifuged (4000 rpm, 20 min), filtrated (0.45
194 µm polyamide membrane filters) and Si was measured by ICP-OES, (ICP-iCAP 6300 DUO,
195 Thermo Fisher SCIENTIFIC GmbH). Analyses of water extractable Si were performed in two
196 lab replicates per sample.
197
198 *2.3.2. Tiron extractable Si ($Si_{Tiron}$), aluminum ($Al_{Tiron}$) and iron ($Fe_{Tiron}$)*
199 The Tiron ($C_6H_4Na_2O_8S_2 \cdot H_2O$) extraction followed the method developed by Biermans &
200 Baert (1977), modified by Kodama & Ross (1991). It has been used to quantify amorphous
201 biogenic and pedogenic Si (Kendrick & Graham 2004), although a partial dissolution of
202 primary minerals is well known (Kodama & Ross 1991, Sauer et al. 2006). The extraction
203 solution was produced by dilution of 31.42 g Tiron with 800 mL of distilled water, followed
204 by addition of 100 mL sodium carbonate solution (5.3 g $Na_2CO_3$ + 100 mL distilled water)
205 under constant stirring. The final pH of 10.5 was reached by adding small volumes of a 4M
206 NaOH-solution. For the extraction 30 mg of dry soil were weighed into 80 mL centrifuge
207 tubes and a 30 mL aliquot of the Tiron solution was added. The tubes were then heated at
208 80°C in a water bath for 1h. The extracted solutions were centrifuged at 4000 rpm for 30
209 min, filtrated (0.45 µm polyamide membrane filters, Whatman NL 17) and Si, Al and Fe
210 measured by ICP-OES. Analyses of Tiron extractable Si, Al and Fe were performed in three
211 lab replicates per sample.
212
213 *2.4. Microscopical analyses of diatoms, sponge spicules and testate amoebae*
214 Fresh soil samples were homogenized by gentle turning of the plastic bags before air drying.
215 Afterwards 2 g of fresh soil were taken per sample and stored in 8 mL of formalin (4 %).
216 Subsequently, biogenic siliceous structures, i.e., diatom frustules, testate amoeba shells and

sponge spicules (Fig. 2A-D), were enumerated in soil suspensions (125 mg fresh mass (FM)) received from serial dilution (1000-125 mg soil in 8 mL of water each) using an inverted microscope (OPTIKA XDS-2, objectives 20:1 and 40:1, equipped with a digital camera OPTIKAM B9).

*2.5. Determination of phytoliths in soil samples*

10 g of dry soil material (<2 mm) were processed in four steps (adapted from Alexandre et al. 1997). First organic matter was oxidized using $H_2O_2$ (30 Vol. %), $HNO_3$ (65 Vol. %) and $HClO_4$ (70 Vol. %) at 80°C until reaction subsides. Secondly, carbonates and Fe oxides were dissolved by boiling the sample in HCl (10 Vol. %) for 30 min. Thirdly, the <2 µm granulometric fraction was removed by dispersion of the remaining solid phase of step 2 with 2 Vol. % sodium hexametaphosphate solution (6–12 h), centrifugation at 1000 rpm for 2–3 min, and subsequent decantation. Finally, the phytoliths were separated by shaking the remaining solid phase of step 3 with 30 mL of sodium polytungstate ($Na_6(H_2W_{12}O_{40})\cdot H_2O$) with a density of 2.3 g $cm^{-3}$ and subsequent centrifugation at 3000 rpm for 10 min.. Afterwards, the supernatant was carefully pipetted and filtered using 5 µm teflon filters. This step was repeated three times. The filter residue was washed with water, bulked, dried at 105°C, and weighted.

*2.6. Quantification of biogenic Si pools*

In general, biogenic siliceous structures consist of hydrated amorphous silica ($SiO_2\cdot nH_2O$). We assumed an average water content of about 10 % for these structures to avoid an overestimation of BSi pools (Mortlock & Froelich 1989).

240 Protophytic Si pools (represented by diatom frustules) were quantified by multiplication of Si
241 contents per frustule with corresponding individual numbers (see Puppe et al. 2016).
242 Protozoic Si pools (represented by testate amoebae) were quantified by multiplication of
243 silica contents of diverse testate amoeba taxa (Aoki et al. 2007) with corresponding
244 individual numbers (living plus dead individuals, for details see Puppe et al. 2014, 2015).
245 Zoogenic Si pools (represented by sponge spicule fragments) were calculated by multiplying
246 volumes ($\mu m^3$) of the found spicule fragments with the density of biogenic Si (2.35 g $cm^{-3}$)
247 and summing up the results. Volume measurements were conducted using a laser scanning
248 microscope (Keyence VK-X110, magnification 200-2.000x) (details in Puppe et al. 2016). For
249 laser scanning microscopy spicule fragments were taken from soil suspensions by
250 micromanipulation, washed in dist. $H_2O$ and placed on clean object slides. After air drying
251 images of spicule fragments were acquired (software Keyence VK-H1XVD) and analyzed
252 (software Keyence VK-H1XAD).
253 Phytogenic Si pools were estimated by multiplying the numbers of found phytoliths with
254 corresponding mean volumes ($\mu m^3$) of phytoliths, multiplying these results with the density
255 of biogenic Si (2.35 g $cm^{-3}$) and summing up the results. Volume measurements with the
256 laser scanning microscope of 30 typical elongate (Fig. 2E) and 30 typical bilobate phytoliths
257 (Fig. 2F) resulted in mean volumes of 3765 $\mu m^3$ and 707 $\mu m^3$, respectively. For laser scanning
258 microscopy extracted phytoliths were placed on clean object slides and images were
259 acquired and analyzed analogous to sponge spicules. For bilobate phytoliths we measured
260 the upper half per phytolith and doubled the result to obtain the corresponding total
261 volume, thus we assumed bilobate phytoliths to be symmetric. We assumed phytoliths to
262 consist of 95 % $SiO_2$ and 5 % other elements, i.e., carbon (Song et al. 2012) and other
263 elements like iron, aluminum or calcium (Buján 2013).

BSi pools (mg $m^{-2}$) were calculated considering bulk density (g $cm^{-3}$), thickness (5 cm) and – for protistic and zoogenic Si pools – water content (% of fresh mass) per soil sample. Silica (M = 60.08 g $mol^{-1}$) pools were converted to Si (M = 28.085 g $mol^{-1}$) pools by multiplication with 28/60 (details in Puppe et al. 2014, 2015, 2016).

*2.7. Plant analyses*

Plant and litter samples of *C. epigejos* and *P. australis* were collected in the summer of 2015. In general, monomeric silicic acid ($H_4SiO_4$) enters the plant via its roots and is carried in the transpiration stream towards transpiration termini. When water evaporates, silicic acid becomes supersaturated and is precipitated as hydrated silica in the form of phytoliths. The vast majority of Si in plants is located at the transpiration termini (e.g., leaves) in the aerial plant parts, while considerably less Si can be found in other plant portions like stems, roots and rhizomes. Sangster (1983), for example, found no significant Si depositions in rhizomes of *P. australis*. Consequently, we only analyzed the aboveground vegetation (including transpiration termini and stems). The collected plant material was washed with distilled water to remove adhering soil minerals and oven-dried at 45°C for 48 hours.

*2.7.1. Total Si content in plant materials*

Plant samples were milled using a knife mill (Grindomix GM 200, Retsch) in two steps: 4.000 rpm for 1 min and then 10.000 rpm for 3 min. Sample aliquots of approximately 100 mg were digested under pressure in PFA digestion vessels using a mixture of 4 mL distilled water, 5 mL nitric acid (65 %), and 1 mL hydrofluoric acid (40 %) at 190°C using a microwave digestion system (Mars 6, CEM). A second digestion step was used to neutralize the hydrofluoric acid with 10 mL of a 4 %-boric acid solution at 150°C. Silicon was measured by

ICP-OES (ICP-iCAP 6300 Duo, Thermo Fisher Scientific GmbH) with an internal standard. To avoid contamination, plastic equipment was used during the complete procedure. Analyses of total Si content were performed in three lab replicates per sample.

*2.7.2. Determination of phytoliths in plants and litter*

Plant material was washed with distilled water and oven-dried at 45°C for 48 hours. Removal of organic matter was conducted by burning the samples in a muffle furnace at 450°C for 12 hours. Next, the material was subject to additional oxidation using 30 % $H_2O_2$ for 12 hours. The obtained material was filtered through a teflon filter with a mesh size of 5 µm. The isolated phytoliths and siliceous cast (>5 µm) were subject to analysis via polarized light microscopy (Nikon ECLIPSE LV100 microscope) for full characteristics. We used laser scanning microscopy for measurements of the surface-area ($\mu m^2$) of the 30 typical bilobate and 30 typical elongated phytoliths used for volume measurements (see 2.6) and calculated corresponding surface-area-to-volume ratios (A/V ratios) as an indicator for the resistibility of these siliceous structures against dissolution. Higher A/V ratios indicate a bigger surface-area available for dissolution processes.

*2.8. Statistical analyses*

Correlations were analyzed using Spearman's rank correlation ($r_s$). Significances in two-sample (n = 2) cases were verified with the Mann-Whitney U-test. For *k*-sample (n > 2) cases the Kruskal-Wallis analysis of variance (ANOVA) was used followed by pairwise multiple comparisons (Dunn's post hoc test). Statistical analyses were performed using software package SPSS Statistics (version 19.0.0.1, IBM Corp.).

## 3. Results

### *3.1. Basic soil parameters*

Soils at the initial state ($t_0$) showed in the upper 5 cm organic carbon contents ($C_{org}$) between 1.1 g $kg^{-1}$ and 4.4 g $kg^{-1}$ in the western section, 0.8 g $kg^{-1}$ and 1.8 g $kg^{-1}$ in the eastern section and 0.2 g $kg^{-1}$ and 3.3 g $kg^{-1}$ in the southern section. This corresponded to mean carbon stocks of 237 g $m^{-2}$ (west), 123 g $m^{-2}$ (east) and 160 g $m^{-2}$ (south, Table 2). After 10 years ($t_{10}$) of ecosystem development the $C_{org}$ stocks increased up to a factor of 3 (396-556 g $m^{-2}$ in the upper 5 cm) compared to corresponding values at $t_0$. This resulted in a surprisingly high mean annual $CO_2$-C sequestration rate of 27-32 g $m^{-2}$ (upper 5 cm). Hereby the largest $C_{org}$ stock changes were found in the western section of the area followed by the eastern section and the southern section (Table 2).

The carbonate contents ($CaCO_3$) at $t_0$ varied between means of 1.0 g $kg^{-1}$ (west), 0.9 g $kg^{-1}$ (east) and 1.8 g $kg^{-1}$ (south). The corresponding stocks were 88 g $m^{-2}$ (west), 91 g $m^{-2}$ (east) and 174 g $m^{-2}$ (south, Table 2). The carbonate pools in the western and eastern section were very similar, while the high carbonate values in the southern section were due to the original soil properties. At $t_{10}$ the distribution of carbonate was as follows: in the western section there was an increase of about 17 % (from 88 g $m^{-2}$ to 101 g $m^{-2}$), in the eastern part a distinct decrease of about 67 % (from 91 g $m^{-2}$ to 30 g $m^{-2}$) was detected and in the southern section again a decrease of about 28 % (from 174 g $m^{-2}$ to 126 g $m^{-2}$) was identified.

At $t_0$ the pH values of the soils showed a range between 7.9 and 8.3 (Table 2) with relatively low variation between the different sections. After 10 years the pH values decreased to 7.1-7.4 in all sections.

336 *3.2. Water and Tiron extractions*

337 The mean water soluble Si ($Si_{H2O}$) contents in the upper 5 cm showed low variation between
338 the different sections at $t_0$: 7.3 mg $kg^{-1}$ (west), 7.2 mg $kg^{-1}$ (east) and 8.6 mg $kg^{-1}$ (south). The
339 corresponding stock values were 0.7 g $m^{-2}$ (west), 0.87 g $m^{-2}$ (east) and 0.84 g $m^{-2}$ (south) for
340 all sections at $t_0$ (Table 2). After 10 years ($t_{10}$) an overall significant increase of $Si_{H2O}$ in each of
341 the different sections compared to $t_0$ was found. The corresponding stock values were 1.7 g
342 $m^{-2}$ (west), 1.5 g $m^{-2}$ (east) and 2.2 g $m^{-2}$ (south, Table 2).

343 At $t_0$ the mean Tiron extractable Si contents in the upper 5 cm varied between 5.5 g $kg^{-1}$
344 (west), 5.2 g $kg^{-1}$ (east) and 4.1 g $kg^{-1}$ (south). The related stock values were 524 g $m^{-2}$ (west),
345 503 g $m^{-2}$ (east) and 399 g $m^{-2}$ (south, Table 2). After 10 years ($t_{10}$) the Tiron extractable Si
346 content showed a slight increase in the western section to 6.5 g $kg^{-1}$ (552 g $m^{-2}$), while the
347 concentration in the eastern section decreased significantly to 2.6 g $kg^{-1}$ (196 g $m^{-2}$, Table 2).
348 In the southern section only a slight decrease to 3.8 g $kg^{-1}$ (317 g $m^{-2}$) was found. The Al and
349 Fe extractable Tiron contents followed the distribution of the Si concentrations with one
350 exception in the western section, where contrary to Si the Al and the Fe contents slightly
351 increased at $t_{10}$ (Table 2). Si/Al ratios ranged between 1.6 and 2.2 at Chicken Creek. Tiron
352 extractable Si and Al fractions as well as Tiron extractable Al and Fe fractions were strongly
353 correlated (Table 3).

354

355 *3.3. Biogenic Si pools in soils*

356 In general, total biogenic Si pools increased in every section after ten years of ecosystem
357 development with statistically significant differences between $t_0$ (11.6 ± 6.5 mg Si $m^{-2}$) and
358 the southern section at $t_{10}$ (96.0 ± 87.2 mg Si $m^{-2}$) (Fig. 3). Total BSi showed strong positive
359 and statistically significant correlations to water soluble Si (Table 3). Phytogenic (phytoliths

360 >5 µm) Si pools ranged from 0-18 mg $m^{-2}$ (mean: 6.6 mg $m^{-2}$) at $t_o$ and significantly increased
361 to means of 20.7 mg $m^{-2}$ (range: 7-52 mg $m^{-2}$) and 12.9 mg $m^{-2}$ (range: 14-15 mg $m^{-2}$) at the
362 eastern and southern section during 10 years, respectively (Fig. 4A). Protophytic Si pools
363 (diatom frustules) ranged from 0-7 mg $m^{-2}$ (mean: 2.6 mg $m^{-2}$) at $t_0$ and increased up to a
364 mean of 47.4 mg $m^{-2}$ (range: 0.1-162 mg $m^{-2}$) at $t_{10}$ (southern section) (Fig. 4B). At $t_0$ no
365 sponge spicules were found with one exception representing an extreme value (12.7 mg $m^{-2}$).
366 After one decade of ecosystem development zoogenic Si pools increased to a maximum
367 of 46 mg $m^{-2}$ at the southern section ($t_{10}$) (Fig. 4C). Protozoic Si pools were zero at $t_0$ with
368 one exception representing an extreme value (1.8 mg $m^{-2}$) and significantly increased to 4.6
369 mg $m^{-2}$ (range: 1-11 mg $m^{-2}$) and 11.5 mg $m^{-2}$ (range: 2-36 mg $m^{-2}$) in the eastern and the
370 southern section at $t_{10}$, respectively (Fig. 4D).
371 At $t_0$ most BSi (>50 %) is represented by phytoliths >5 µm followed by diatom frustules,
372 sponge spicules and testate amoeba shells (Fig. 5). After ten years of ecosystem
373 development the proportion of the different BSi pools to total BSi changed. While the
374 proportion of protozoic Si pools increased in all sections at $t_{10}$, the other BSi pools showed
375 more variable changes over time. The proportion of phytogenic Si pools either increased
376 (western section) or decreased (eastern and southern sections). In contrast, the proportion
377 of protophytic Si pools decreased at the western section and increased in the eastern and
378 southern sections. The proportion of zoogenic Si pools decreased in the western and eastern
379 sections, but increased slightly in the southern section at $t_{10}$.
380
381 *3.4. Phytoliths and total Si content in plant materials*
382 The total content of Si was determined for two Si accumulating plant species *Calamagrostis*
383 *epigejos* and *Phragmites australis* dominating distinct catchment sections. For *C. epigejos*

384 the mean total content of Si was 2.25 % (range: 1.8-3.1 %), whereas for *P. australis* a mean
385 total Si content of 2.70 % (range: 2.0-3.2 %) was determined (Fig. 6A, B). For litter we found
386 mean total Si contents of 3.1 % (range: 2.8-3.3 %) and 2.9 % (range: 1.7-3.2 %) for *C. epigejos*
387 and *P. australis*, respectively.
388 Phytoliths >5 µm were also isolated from both plants; for *C. epigejos* the mean extracted
389 phytolith content was 0.37 % (range: 0.31-0.46 %), whereas for *P. australis* a mean phytolith
390 content of 0.43 % (range: 0.37-0.50 %) was determined (Fig. 6A, B), i.e., related to the total
391 Si content of plants 16.4 % and 15.9 % of phytogenic Si were represented by extracted
392 phytoliths >5 µm in *C. epigejos* and *P. australis*, respectively. Thus, small-scale (<5 µm)
393 and/or fragile (siliceous structures mostly thinner than 5 µm, but up to several hundred
394 micrometers long, Fig. 7) phytogenic Si represented 83.6 % and 84.1 % of total phytogenic Si
395 in *C. epigejos* and *P. australis*, respectively. Mean extracted phytolith contents in plant litter
396 were 0.47 % (range: 0.35-0.70 %) and 0.51 % (range: 0.41-0.59 %) for *C. epigejos* and *P.*
397 *australis*, respectively.
398 Surface-areas of 30 typical bilobate and 30 typical elongate phytoliths were in a range of 216
399 $\mu m^2$ to 3,730 $\mu m^2$ and 2,302 $\mu m^2$ to 22,203 $\mu m^2$, respectively (Table 4). The corresponding
400 volumes of bilobate and elongate phytoliths were in a range of 36 $\mu m^3$ to 2,046 $\mu m^3$ and 390
401 $\mu m^3$ to 14,649 $\mu m^3$, respectively. Surface-to-volume ratios of bilobate and elongate
402 phytoliths were in a range of 0.7 to 9.8 and 0.6 to 5.9 with means of 2.8 and 2.6,
403 respectively.
404
405 *3.5. BSi and Si fractions under* Calamagrostis epigejos *and* Phragmites australis
406 Water soluble Si fractions increased by 99 % and 163 %, total BSi by 281 % and 660 % after
407 ten years of ecosystem development in soils under *C. epigejos* and *P. australis*, respectively

(Fig. 6A, B). In contrast, $Si_{Tiron}$ decreased by 42 % and 1.4 % from $t_0$ to $t_{10}$ in soils under *C. epigejos* and *P. australis*, respectively. If we assume mean dry biomasses of 115 g $m^{-2}$ and 186 g $m^{-2}$ for *C. epigejos* and *P. australis* (M. Wehrhan, pers. comm., 2017) about 2.6 g Si $m^{-2}$ and 5.0 g Si $m^{-2}$ are stored in the aboveground biomass at Chicken Creek at $t_{10}$, respectively. For litter of *C. epigejos* and *P. australis* (mean dry biomasses of 59 g $m^{-2}$ and 94 g $m^{-2}$ at $t_{10}$, M. Wehrhan, pers. comm., 2017) we calculated corresponding pools of about 1.8 g Si $m^{-2}$ and 2.7 g Si $m^{-2}$ at $t_{10}$, respectively.

## 4. Discussion

### *4.1. Drivers of short-term changes of water soluble Si at Chicken Creek*

In general, weathering of silicates represents the ultimate source of $Si(OH)_4$ in terrestrial biogeosystems in the long term (Berner 2003). In this context, the long-term accumulation of BSi can influence the total amorphous (Tiron extractable) Si as it is known from forested catchments or old chronosequence soils (Conley et al. 2008, Kendrick & Graham 2004, Saccone et al. 2008). Contrary, short-term changes of BSi pools likely do not influence Tiron extractable Si in initial soils (total BSi represents only 0.002-0.03 % of Tiron extractable Si at Chicken Creek). Thus, the major proportion of Tiron extractable Si at Chicken Creek seems to be of pedogenic origin (e.g., Si included in Al/Fe oxides/hydroxides). This is supported by relatively low Si/Al ratios (<5) indicating a minerogenic origin of Tiron extractable Si instead of BSi as a source of $Si_{Tiron}$ (Bartoli & Wilding 1980). We further exclude changes of Tiron extractable Si as the main driver of water soluble Si at Chicken Creek in the short term, because i) $Si_{Tiron}$ and $Si_{H2O}$ showed no statistical relationship at all and ii) a significant change of the Tiron extractable Si fraction occurred only in the eastern section, whereas in the western and southern section $Si_{Tiron}$ did not change significantly over time. We assume that

these changes of $Si_{Tiron}$ in the eastern section are related to abiotic conditions (soil pH, conductivity, skeleton content, proportions of sand, silt and clay, concentration of organic and inorganic carbon), which were slightly different to the conditions of the western section already at $t_0$ (Gerwin et al. 2010). Furthermore, we excluded atmospheric inputs as potential drivers of short-term changes of water soluble Si at Chicken Creek. On the one hand, dust depositions (dry deposition) at Chicken Creek are very low (73-230 mg $m^{-2}$ $d^{-1}$) and only slightly above the annual average (70-90 mg $m^{-2}$ $d^{-1}$) measured in the state of Brandenburg (Wanner et al. 2015). On the other hand, the total input of Si (as a lithogenic element) by precipitation (wet deposition) is negligible as well (<1 kg Si $ha^{-1}$ $yr^{-1}$, Sommer et al. 2013).

Our results indicate a strong relationship between water soluble Si and total BSi. In this context, two different causal chains can be discussed: Either $SiO_2$-synthesizing organisms are drivers of the amount of $Si(OH)_4$ in the soil or – *vice versa* – the amount of water soluble Si in the soils is the main driver of $SiO_2$-synthesizing organisms as biosilicification is limited by $Si(OH)_4$. Laboratory studies, for example, revealed that $SiO_2$-synthesizing organisms, i.e., testate amoebae, can deplete the amount of $Si(OH)_4$ in culture media due to biosilicification (Aoki et al. 2007, Wanner et al. 2016). However, Wanner et al. (2016) also showed that culture growth of $SiO_2$-synthesizing testate amoebae was dependent on Si concentration in the culture media. Furthermore, *in situ* analyses showed that marine diatom blooms can deplete $Si(OH)_4$ concentrations in the oceans (Hildebrand 2008). In forested biogeosystems Puppe et al. (2015) found high individual numbers of $SiO_2$-synthesizing testate amoebae at study sites with low amounts of $Si(OH)_4$ and *vice versa*. However, it is unlikely that testate amoebae depleted amounts of $Si(OH)_4$ at these sites, because corresponding protozoic Si pools are relatively small compared to phytogenic ones (Puppe et al. 2015, Sommer et al. 2013). Regarding vegetation and corresponding phytogenic Si pools their influence on the

456 amount of $Si(OH)_4$ in soils has been shown in several studies (e.g., Bartoli 1983, Farmer et al.
457 2005, Sommer et al. 2013). On the other hand, phytolith production is probably more
458 influenced by the phylogenetic position of a plant than by environmental factors like
459 temperature or Si availability (Hodson et al. 2005, Cooke & Leishman 2012).
460 From our results and the discussion above we conclude short-term changes of water soluble
461 Si to be mainly driven by BSi. However, total BSi represents only small proportions of water
462 soluble Si at $t_0$ (<2 %) and $t_{10}$ (<4.5 %). From this result the question arises, where does the
463 major part of the increase in water soluble Si at Chicken Creek come from? We will discuss
464 this question in the subsection (4.2.) below.
465
466 *4.2. Sources of water soluble Si at Chicken Creek*
467 From former results of BSi analyses in forested biogeosystems, we assumed the phytogenic
468 Si pool to be the most prominent in size. In this context, results of Sommer et al. (2013) and
469 Puppe et al. (2015) showed that phytogenic Si pools in soils of forested biogeosystems were
470 up to several hundred times larger than protozoic Si pools. However, phytogenic Si pools in
471 soils are surprisingly small compared to other BSi pools at Chicken Creek. Our findings can be
472 attributed to at least two reasons. Firstly, phytogenic Si is stored in a developing organic
473 litter layer where it is temporarily protected against dissolution and secondly, the used
474 methods were not able to accurately quantify the total phytogenic Si pool, but only the
475 larger (>5 μm) and stable part.
476 Total Si and phytolith contents of litter samples at Chicken Creek did not differentiate from
477 total Si and phytolith contents of plants. This fact indicates that litter decomposition and
478 related Si release into the subjacent soil are relatively slow processes and we interpret our
479 findings as a hint for a developing compartment of dead plant tissue above the mineral soil

surface. Esperschütz et al. (2013) showed in a field experiment in initial soils near Chicken Creek that after 30 weeks only 50 % of the litter of *C. epigejos* were degraded, whereby degradation rates were highest in the first four weeks. Estimations of biomasses of *C. epigejos* and *P. australis* at Chicken Creek via remote sensing with an unmanned aerial system showed that the relation between phytogenic Si pools plant biomass and litter biomass is almost the same for both plant species (factor about 1.5, based on the total area of Chicken Creek), i.e., Si in the plants was about one third higher than in litter (M. Wehrhan, pers. comm., 2017, manuscript in preparation). At the sampling points about 1.8 g Si $m^{-2}$ and 2.7 g Si $m^{-2}$ were stored in the litter of *C. epigejos* and *P. australis* at $t_{10}$, respectively, which is in the range of published data for annual Si input through litterfall in a short grass steppe (2.2-2.6 g Si $m^{-2}$ per year, Blecker et al. 2006).

Altogether, these results clearly underline our interpretation of a developing organic layer where litter accumulates and phytogenic Si is temporarily stored and protected against dissolution, thus Si release is delayed biologically controlled as it can be observed at forested biogeosystems (Sommer et al. 2013). The Si pools in the aboveground biomass of *C. epigejos* (2.6 g Si $m^{-2}$) and *P. australis* (5.0 g Si $m^{-2}$) at Chicken Creek at $t_{10}$ are comparable to reported values of Great Plains grasslands (2.2-6.7 g Si $m^{-2}$ in the aboveground biomass) (Blecker et al. 2006) and reach about 30 % (*C. epigejos*) or 59 % (*P. australis*) of published data for a beech forest (8.5 g Si $m^{-2}$ in the aboveground biomass of *Fagus sylvatica* trees) in northern Brandenburg, Germany (Sommer et al. 2013), after (only) ten years of ecosystem development.

Regarding methodological shortcomings of the used phytolith extraction procedure there are several aspects to be discussed. Wilding & Drees (1971), for example, showed that about 72 % of leaf phytoliths of American beech (*Fagus grandifolia*) are smaller than 5 µm. This is

in accordance with our findings. Phytoliths >5 µm only amounted to about 16 % of total Si contents of plant materials of *C. epigejos* and *P. australis*, thus about 84 % of phytogenic Si (<5 µm and /or fragile phytogenic Si structures) are not quantified by the used phytolith extraction method. Watteau & Villemin (2001) found even smaller (5-80 nm) spherical grains of pure silica in leaf residues in topsoil samples of a forested biogeosystem. In addition, silica depositions can be found in intercellular spaces or in an extracellular (cuticular) layer (Sangster et al. 2001), whereat no recognizable phytoliths are formed. These structures might be too fragile for preservation in soils and are likely lost to a great extent in the used phytolith extraction procedure due to dissolution. Meunier et al. (2017) analyzed different phytolith morphotypes, e.g, silica bodies originating from cells of the upper epidermis, silica casts of trichomes or parenchyma/collenchyma cells, of durum wheat plant shoots. They found fragile sub-cuticular silica plates (2-4 µm thick, up to several hundred micrometers long and wide) to be the second most common phytolith morphotype. This is corroborated by our own findings as the biggest part (about 84 %) of total plant Si is represented by small-scale (<5 µm) and/or fragile phytogenic Si in *C. epigejos* and *P. australis*. If we assume that total Si contents of plants at Chicken Creek are one-to-one reflected by phytogenic Si pools in soils we can easily calculate these small-scale and fragile pools resulting in about 130 mg $m^{-2}$ and 100 mg $m^{-2}$ (84 % of total, i.e., 156 mg $m^{-2}$ and 119 mg $m^{-2}$, phytogenic Si each) under *C. epigejos* and *P. australis*, respectively. These calculated phytogenic Si pools are about 13 (diatom frustules), 38 (testate amoeba shells) and 45 (sponge spicules) or 3 (diatom frustules) and 10 (testate amoeba shells, sponge spicules) times bigger than the other BSi pools at *C. epigejos* and *P. australis* sampling points, respectively. If we further assume an input of this phytogenic Si for at least seven years (Zaplata et al. 2010) phytogenic Si might be the main driver of short-term changes of water soluble Si at Chicken Creek. This

528 is supported by relatively high surface-to-volume ratios of bilobate and elongate phytoliths.
529 These ratios are about three times higher compared to ratios of other biogenic siliceous
530 structures, i.e., testate amoeba shells, diatom frustules and sponge spicules.
531 In addition, Si pools represented by single siliceous platelets of testate amoeba shells have
532 to be considered as well as these platelets can be frequently found in freshwater sediments,
533 for example (Douglas & Smol 1987, Pienitz et al. 1995). Unfortunately, there is no
534 information on the quantity of such platelet pools in soils available, but it can be assumed
535 that these platelets can be frequently found in soils as they are used by some testate
536 amoeba genera (e.g., *Schoenbornia*, *Heleopera*) for shell construction (Meisterfeld 2002,
537 Schönborn et al. 1987). In general, it can be assumed that phytogenic Si structures <5 µm
538 and single testate amoeba platelets (about 3-12 µm in diameter, Douglas & Smol 1987) are
539 highly reactive due to their relatively high surface/volume ratios. However, to the best of our
540 knowledge there is no publication available dealing with corresponding physicochemical
541 analyses or dissolution kinetics of these siliceous structures. In general, experiments with
542 phytoliths (>5 µm) showed that surface-areas and related dissolution susceptibilities are, for
543 example, age-related due to changes in specific surface areas and the presence of organic
544 matter bound to the surface of phytoliths (Fraysse et al. 2006, 2009).
545
546 **5. Conclusions**
547 Decadal changes of water soluble Si at Chicken Creek are mainly driven by BSi, thus Si cycling
548 is biologically controlled already at the very beginning of ecosystem development. In this
549 context, especially phytogenic Si plays a prominent role. However, a developing organic layer
550 (L horizon) at the soil surface temporarily protects phytogenic Si against dissolution, because
551 phytogenic Si is still incorporated in plant structural elements (tissues). In consequence a

552 delaying biogenic Si pool is built up and Si release into the soil is retarded. Furthermore,
553 established phytolith extraction methods alone are not suitable to quantify total phytogenic
554 Si pools as phytoliths >5 µm seem to be only a minor part of this pool (about 16 % in the
555 current study). In general, information on small-scale (<5 µm) and/or fragile phytogenic Si
556 structures are urgently needed as they seem to represent the biggest and most reactive Si
557 pool in soils, thus the most important driver of Si cycling in terrestrial biogeosystems. Future
558 work should focus on i) the quantification of this pool, ii) physicochemical analyses of its
559 components, and (iii) their dissolution kinetics in lab experiments. The combination of
560 modern microscopical (SEM-EDX, laser scanning microscopy) (this study, Puppe et al. 2016,
561 Sommer et al. 2013) and spectroscopical (FTIR and micro-FTIR spectroscopy) (Liu et al. 2013,
562 Loucaides et al. 2010, Rosén et al. 2010) methods might introduce new insights in this field.
563
564 **Acknowledgements**
565 This study has been financed by the DFG project 'Spatiotemporal dynamics of biogenic Si
566 pools in initial soils and their relevance for desilication' (SO 302/7-1). Many thanks to
567 Christian Buhtz and Reneé Ende for their excellent laboratory support. We would like to
568 thank the members of the 'Chicken Creek project' at BTU Cottbus-Senftenberg for providing
569 soil samples from 2005 and organizational support. Vattenfall Europe Mining AG provided
570 the research site. This study is a contribution to the Transregional Collaborative Research
571 Centre 38 (SFB/TRR 38) financially supported by the German Research Council (DFG, Bonn)
572 and the Brandenburg Ministry of Science, Research and Culture (MWFK, Potsdam). Last but
573 not least we would like to thank the anonymous reviewers for their very helpful comments
574 on our manuscript.
575

576 **References**

577 Alexandre, A., Meunier, J. D., Colin, F., Koud, J. M., 1997. Plant impact on the biogeochemical
578 cycle of silicon and related weathering processes. *Geochimica et Cosmochimica Acta* 61, 677-
579 682.

580 Aoki, Y., Hoshino, M., Matsubara, T., 2007. Silica and testate amoebae in a soil under pine–
581 oak forest. *Geoderma* 142, 29-35.

582 Barão, L., Clymans, W., Vandevenne, F., Meire, P., Conley, D.J., Struyf, E., 2014. Pedogenic
583 and biogenic alkaline-extracted silicon distributions along a temperate land-use gradient.
584 *Eur. J. Soil Sci.* 65, 693-705.

585 Bartoli, F., 1983. The biogeochemical cycle of silicon in two temperate forest ecosystems.
586 Environ. *Biogeochem. Ecol. Bull.* 35, 469-476.

587 Bartoli, F. & L. P. Wilding, 1980. Dissolution of biogenic opal as a function of its physical and
588 chemical properties. *Soil Science Society of America Journal* 44, 873-878.

589 Berner, R. A., 2003. The long-term carbon cycle, fossil fuels and atmospheric composition.
590 *Nature* 426, 323-326.

591 Biermans, V., Baert, L., 1977. Selective extraction of the amorphous Al, Fe and Si oxides using
592 an alkaline Tiron solution. *Clay Miner*., 12, 127-135.

593 Blecker, S. W., McCulley, R. L., Chadwick, O. A. & Kelly, E. F., 2006. Biologic cycling of silica
594 across a grassland bioclimosequence. *Global Biogeochemical Cycles* 20, GB3023.

595 Buján, E., 2013. Elemental composition of phytoliths in modern plants (Ericaceae).
596 *Quaternary International* 287, 114-120.

597 Clarke, J., 2003. The occurrence and significance of biogenic opal in the regolith. *Earth-Sci.*
598 *Rev.* 60, 175-194.

599 Clymans, W., Struyf, E., Govers, G., Vandevenne, F., Conley, D.J., 2011. Anthropogenic impact
600 on amorphous silica pools in temperate soils. *Biogeosciences* 8, 2281-2293.

601 Conley, D. J., G. E. Likens, D. C. Buso, L. Saccone, S. W. Bailey & C. E. Johnson, 2008.
602 Deforestation causes increased dissolved silicate losses in the Hubbard Brook Experimental
603 Forest. *Global Change Biology* 14, 2548-2554.

604 Cooke, J. & Leishman, M. R., 2012. Tradeoffs between foliar silicon and carbon-based
605 defences: evidence from vegetation communities of contrasting soil types. *Oikos* 121, 2052-
606 2060.

607 Creevy, A.L., Fisher, J., Puppe, D., Wilkinson, D.M., 2016. Protist diversity on a nature reserve
608 in NW England – with particular reference to their role in soil biogenic silicon pools.
609 *Pedobiologia* 59, 51-59.

610 DIN ISO 1039, 1997. Bodenbeschaffenheit: Bestimmung des pH-Wertes. Deutsches Institut
611 für Normung, Beuth, Berlin.

612 Douglas, M.S. & J.P. Smol, 1987. Siliceous protozoan plates in lake sediments. *Hydrobiologia*
613 154, 13-23.

614 Dürr, H.H., Meybeck, M., Hartmann, J., Laruelle, G.G., Roubeix, V., 2011. Global spatial
615 distribution of natural riverine silica inputs to the coastal zone. *Biogeosciences* 8, 597-620.

616 Ehrlich, H., Demadis, K.D., Pokrovsky, O.S., Koutsoukos, P.G., 2010. Modern views on
617 desilicification: biosilica and abiotic silica dissolution in natural and artificial environments.
618 *Chem. Rev.* 110, 4656-4689.

619 Epstein, E., 2009. Silicon: its manifold roles in plants. *Annals of Applied Biology* 155, 155-160.

620 Esperschütz, J., Zimmermann, C., Dümig, A., Welzl, G., Buegger, F., Elmer, M., Munch, J. C.,
621 Schloter, M., 2013. Dynamics of microbial communities during decomposition of litter from
622 pioneering plants in initial soil ecosystems. *Biogeosciences* 10, 5115-5124.

623 Farmer, V. C., Delbos, E., Miller, J. D., 2005. The role of phytolith formation and dissolution in
624 controlling concentrations of silica in soil solutions and streams. *Geoderma* 127, 71-79.

625 Fraysse, F., Pokrovsky, O. S., Schott, J., Meunier, J. D., 2006. Surface properties, solubility and
626 dissolution kinetics of bamboo phytoliths. *Geochimica et Cosmochimica Acta* 70, 1939-1951.

627 Fraysse, F., Pokrovsky, O. S., Schott, J., Meunier, J. D., 2009. Surface chemistry and reactivity
628 of plant phytoliths in aqueous solutions. *Chemical Geology* 258, 197-206.

629 Frings, P. J., Clymans, W., Jeppesen, E., Lauridsen, T. L., Struyf, E., Conley, D. J., 2014. Lack of
630 steady-state in the global biogeochemical Si cycle: emerging evidence from lake Si
631 sequestration. *Biogeochemistry* 117, 255-277.

632 Gerwin, W., Schaaf, W., Biemelt, D., Fischer, A., Winter, S., Hüttl, R.F., 2009. The artificial
633 catchment 'Chicken Creek' (Lusatia, Germany) – A landscape laboratory for interdisciplinary
634 studies of initial ecosystem development. *Ecol. Eng.* 35, 1786-1796.

635 Gerwin, W., Schaaf, W., Biemelt, D., Elmer, M., Maurer, T., Schneider, A., 2010. The Artificial
636 catchment 'Hühnerwasser' (Chicken Creek): construction and initial properties. Ecosystem
637 Development 1 (edited by Hüttl, R.F., Schaaf, W., Biemelt, D., Gerwin, W), Brandenburg
638 University of Technology Cottbus-Senftenberg, Germany.

639 Hildebrand, M., 2008. Diatoms, biomineralization processes, and genomics. *Chemical*
640 *Reviews* 108, 4855-4874.

641 Hodson, M. J., White, P. J., Mead, A., Broadley, M. R., 2005. Phylogenetic variation in the
642 silicon composition of plants. *Annals of Botany* 96, 1027-1046.

643 Keller, C., Guntzer, F., Barboni, D., Labreuche, J., Meunier, J.D., 2012. Impact of agriculture
644 on the Si biogeochemical cycle: input from phytolith studies. *C. R. Geosci.* 344, 739-746.

645 Kendrick, K. J., Graham, R.C., 2004. Pedogenic silica accumulation in chronosequence soils,
646 Southern California. *Soil Sci. Soc. Am. J.* 68, 1295-1303.

647 Kodama, H., Ross, G.J., 1991. Tiron dissolution method used to remove and characterize
648 inorganic components in soils. *Soil Sci. Soc. Am. J.* 55, 1180-1187.

649 Kendzia, G., Reißmann, R., Neumann, T., 2008. Targeted development of wetland habitats
650 for nature conservation fed by natural inflow in the post-mining landscape of Lusatia. *World*
651 *Min.* 60, 88-95.

652 Liu, X., S.M. Colman, E.T. Brown, E.C. Minor & H. Li, 2013. Estimation of carbonate, total
653 organic carbon, and biogenic silica content by FTIR and XRF techniques in lacustrine
654 sediments. *Journal of Paleolimnology* 50, 387-398.

655 Loucaides, S., T. Behrends & P. Van Cappellen, 2010. Reactivity of biogenic silica: Surface
656 versus bulk charge density. *Geochimica et Cosmochimica Acta* 74, 517-530.

657 Ma, J. F. & N. Yamaji, 2008. Functions and transport of silicon in plants. *Cellular and*
658 *Molecular Life Sciences* 65, 3049-3057.

659 McKeague, J.A., Cline, M.G., 1963. Silica in soil solutions I. The form and concentration of
660 dissolved silica in aqueous extracts of some soils. *Can. J. Soil Sci.* 43, 70-82.

661 Meisterfeld, R. (2002). Order Arcellinida Kent, 1880. The illustrated guide to the Protozoa
662 (ed. by J. J. Lee, G. F. Leedale & P. Bradbury), pp. 827-860. Society of Protozoologists,
663 Lawrence, KS, USA.

664 Meunier, J.D., Colin, F., Alarcon, C., 1999. Biogenic silica storage in soils. *Geology* 27, 835-
665 838.

666 Meunier, J. D., Barboni, D., Anwar-ul-Haq, M., Levard, C., Chaurand, P., Vidal, V., Grauby, O.,
667 Huc, R., Laffont-Schwob, I., Rabier, J., Keller, C., 2017. Effect of phytoliths for mitigating
668 water stress in durum wheat. *New Phytologist*, doi: 10.1111/nph.14554.

669 Mortlock, R.A., Froelich, P.N., 1989. A simple method for the rapid determination of biogenic
670 opal in pelagic marine sediments. *Deep-Sea Res.* 36, 1415-1426.

671 Pienitz, R., M.S. Douglas, J.P. Smol, P. Huttunen & J. Meriläinen, 1995. Diatom, chrysophyte
672 and protozoan distributions along a latitudinal transect in Fennoscandia. *Ecography* 18, 429-
673 439.

674 Puppe, D., Kaczorek, D., Wanner, M., Sommer, M., 2014. Dynamics and drivers of the
675 protozoic Si pool along a 10-year chronosequence of initial ecosystem states. *Ecol. Eng.* 70,
676 477-482.

677 Puppe, D., Ehrmann, O., Kaczorek, D., Wanner, M., Sommer, M., 2015. The protozoic Si pool
678 in temperate forest ecosystems – Quantification, abiotic controls and interactions with
679 earthworms. *Geoderma* 243-244, 196-204.

680 Puppe, D., Höhn, A., Kaczorek, D., Wanner, M., Sommer, M., 2016. As Time Goes By –
681 Spatiotemporal Changes of Biogenic Si Pools in Initial Soils of an Artificial Catchment in NE
682 Germany. *Appl. Soil Ecol.* 105, 9-16.

683 Rosén, P., H. Vogel, L. Cunningham, N. Reuss, D.J. Conley & P. Persson, 2010. Fourier
684 transform infrared spectroscopy, a new method for rapid determination of total organic and
685 inorganic carbon and biogenic silica concentration in lake sediments. *Journal of*
686 *Paleolimnology* 43, 247-259.

687 Russell, D.J., Hohberg, K., Elmer, M., 2010. Primary colonisation of newly formed soils by
688 actinedid mites. *Soil Org.* 82, 237-251.

689 Saccone, L., D. J. Conley, G. E. Likens, S. W. Bailey, D. C. Buso & C. E. Johnson, 2008. Factors
690 that control the range and variability of amorphous silica in soils in the Hubbard Brook
691 Experimental Forest. *Soil Science Society of America Journal* 72, 1637-1644.

692 Sangster, A. G., 1983. Anatomical features and silica depositional patterns in the rhizomes of
693 the grasses *Sorghastrum nutans* and *Phragmites australis*. *Canadian Journal of Botany* 61,
694 752-761.

695 Schönborn, W., W. Petz, M. Wanner & W. Foissner (1987). Observations on the Morphology
696 and Ecology of the Soil-Inhabiting Testate Amoeba *Schoenbornia humicola* (Schönborn,
697 1964) Decloitre, 1964 (Protozoa, Rhizopoda). *Archiv für Protistenkunde* 134, 315-330.

698 Sangster, A. G., Hodson, M. J. & H. J. Tubb (2001). Silicon deposition in higher plants, pp. 85-
699 113, in: Datnoff, L. E., Snyder, G. H. & G. H. Korndörfer (eds.). Silicon in agriculture (Vol. 8).
700 Elsevier, Amsterdam, The Netherlands.

701 Sauer, D., Saccone, L., Conley, D.J., Herrmann, L., Sommer, M., 2006. Review of
702 methodologies for extracting plant-available and amorphous Si from soils and aquatic
703 sediments. *Biogeochem.* 80, 89-108.

Schaaf, W., Biemelt, D., Hüttl, R.F., 2010. Initial development of the artificial catchment 'Chicken Creek' – monitoring program and survey 2005-2008. Ecosystem Development 2 (edited by Hüttl, R.F., Schaaf, W., Biemelt, D., Gerwin, W.), 194 pp.

Schachtschabel, P., Heinemann, C.G., 1967. Wasserlösliche Kieselsäure in Lößböden. *Z. Pflanzenern. Bodenk.* 118, 22-35.

Schlichting, E., Blume, H.P., Stahr, K., 1995. Soils Practical (in German), Blackwell, Berlin, Wien, Germany, Austria.

Schneider, A., Gerke, H. H., Maurer, T., Nenov, R., 2013. Initial hydro-geomorphic development and rill network evolution in an artificial catchment. *Earth Surface Processes and Landforms* 38, 1496-1512.

Sommer, M., Kaczorek, D., Kuzyakov, Y., Breuer, J., 2006. Silicon pools and fluxes in soils and landscapes—a review. *J. Plant Nutr. Soil Sci.* 169, 310-329.

Sommer, M., Jochheim, H., Höhn, A., Breuer, J., Zagorski, Z., Busse, J., Barkusky, D., Meier, K., Puppe, D., Wanner, M., Kaczorek, D., 2013. Si cycling in a forest biogeosystem - the importance of transient state biogenic Si pools. *Biogeosciences* 10, 4991-5007.

Song, Z., Wang, H., Strong, P. J., Li, Z., Jiang, P., 2012. Plant impact on the coupled terrestrial biogeochemical cycles of silicon and carbon: implications for biogeochemical carbon sequestration. *Earth-Science Reviews* 115, 319-331.

Street-Perrott, F. A., Barker, P. A., 2008. Biogenic silica: a neglected component of the coupled global continental biogeochemical cycles of carbon and silicon. *Earth Surface Processes and Landforms* 33, 1436-1457.

Struyf, E., Conley, D.J., 2012. Emerging understanding of the ecosystem silica filter. *Biogeochemistry* 107, 9-18.

727 Struyf, E., Smis, A., Van Damme, S., Garnier, J., Govers, G., Van Wesemael, B., Conley, D.J,
728 Batelaan, O., Frot, E., Clymans, W., Vandevenne, F., Lancelot, C., Goos, P., Meire, P., 2010.
729 Historical land use change has lowered terrestrial silica mobilization. *Nature*
730 *Communications* 1, 129.

731 Tréguer, P.J., De La Rocha, C.L., 2013. The world ocean silica cycle. *Ann. Rev. Mar. Sci.* 5, 477-
732 501.

733 Tréguer, P., Pondaven, P., 2000. Global change: silica control of carbon dioxide. *Nature* 406,
734 358-359.

735 Vandevenne, F. I., Barão, L., Ronchi, B., Govers, G., Meire, P., Kelly, E. F., Struyf, E., 2015.
736 Silicon pools in human impacted soils of temperate zones. *Global Biogeochemical Cycles* 29,
737 1439-1450.

738 Wanner, M., Elmer, M., 2009. “Hot spots” on a new soil surface – how do testate amoebae
739 settle down? *Acta Protozoologica* 48, 281-289.

740 Wanner, M., Elmer, M., Sommer, M., Funk, R., Puppe, D., 2015. Testate amoebae colonizing
741 a newly exposed land surface are of airborne origin. *Ecological Indicators* 48, 55-62.

742 Wanner, M., Seidl-Lampa, B., Höhn, A., Puppe, D., Meisterfeld, R., Sommer, M., 2016.
743 Culture growth of testate amoebae under different silicon concentrations. *European Journal*
744 *of Protistology* 56, 171-179.

745 Watteau, F., Villemin, G., 2001. Ultrastructural study of the biogeochemical cycle of silicon in
746 the soil and litter of a temperate forest. *European Journal of Soil Science* 52, 385-396.

747 Wilding, L. P., Drees, L. R., 1971. Biogenic opal in Ohio soils. *Soil Science Society of America*
748 *Journal* 35, 1004-1010.

749 Zaplata, M.K., A. Fischer & S. Winter, 2010. Vegetation dynamics, in: Ecosystem
750 development 2 (edited by Schaaf, W., Biemelt, D., Hüttl, R.F.), Brandenburg University of
751 Technology Cottbus-Senftenberg, Germany.

752

753

754

755

756

757

758

759

760

761

762

763

764

765

766

767

768

769

**Figures and Figure captions**

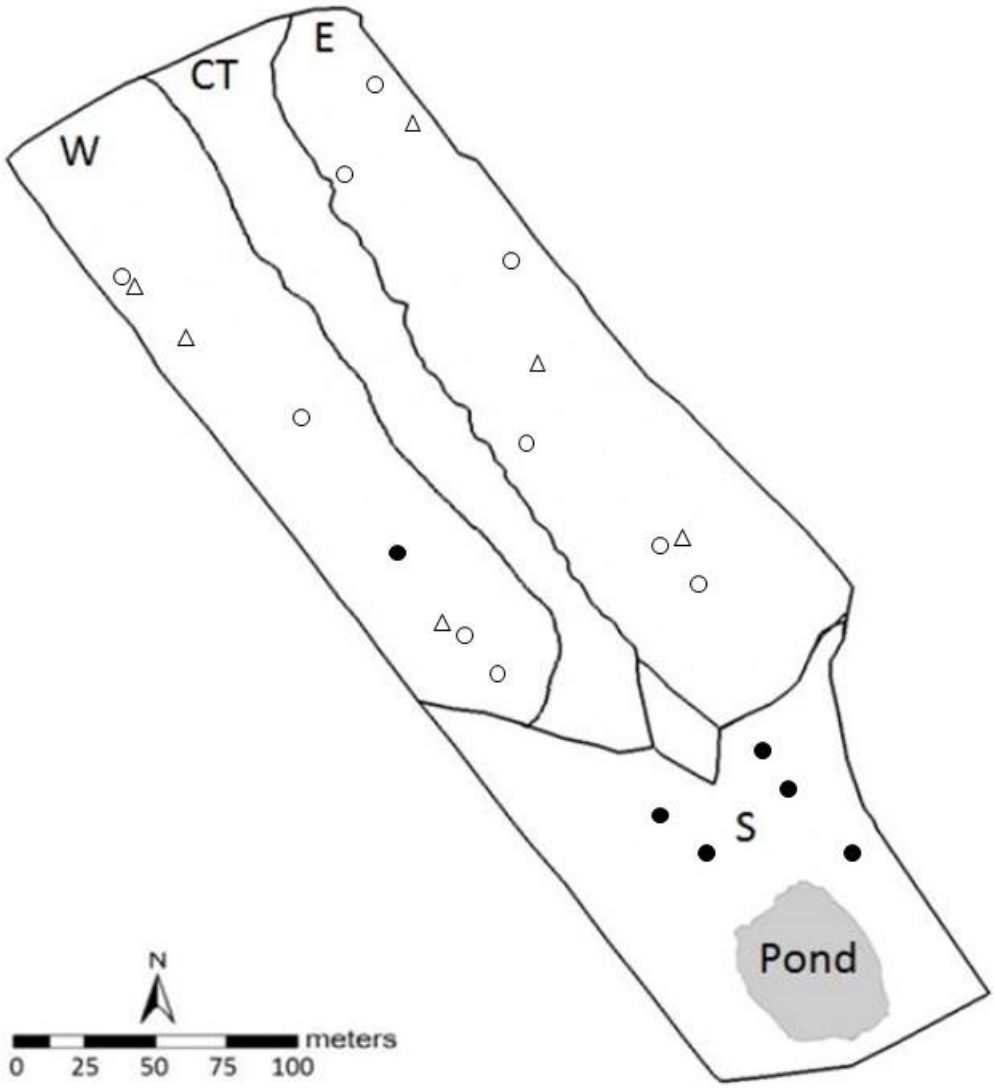


**Fig. 1.** Map of Chicken Creek (W = western section, CT = central trench, E = eastern section, S = southern section with pond). Triangles indicate the sampling points used for BSi analyses at $t_0$ (n = 6). Circles indicate the sampling points used for measurements of soil parameters (at $t_0$ and $t_{10}$) and plant analyses (only at $t_{10}$) (W, n = 5; E, n = 6; S, n = 5). Empty and filled circles represent sampling points where *Calamagrostis epigejos* and *Phragmites australis* became dominant. Note that the size of sampling points is not to scale.

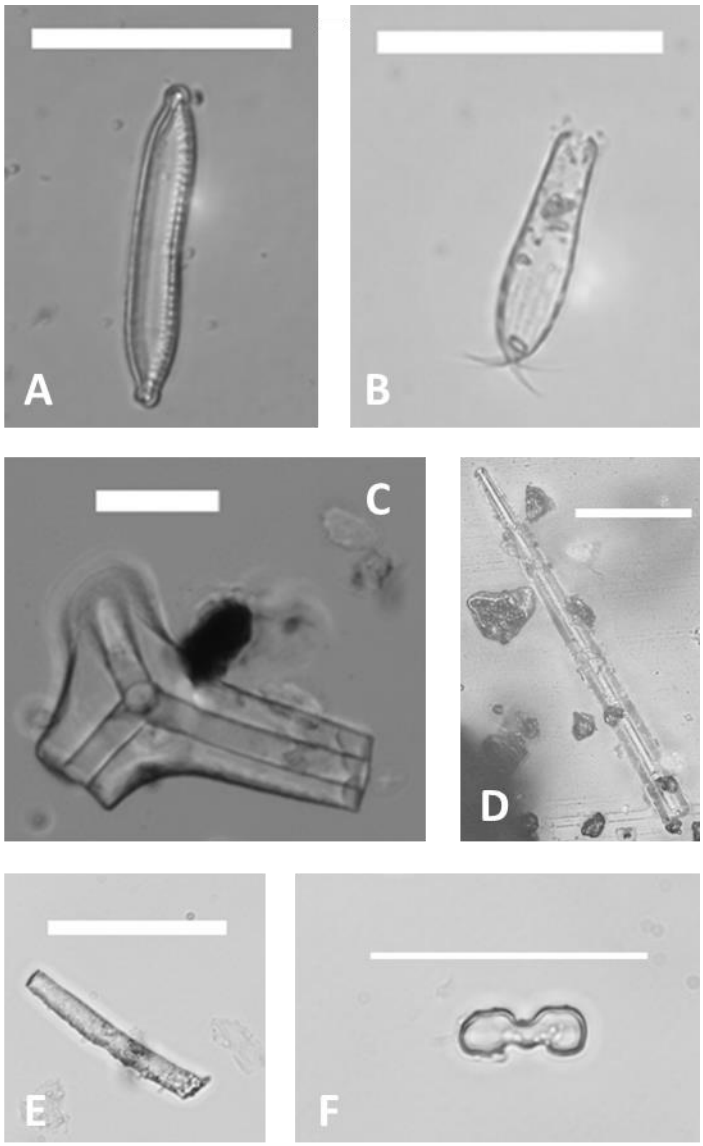


778

779 **Fig. 2.** Micrographs (light microscope) of biogenic silica structures found at Chicken Creek. A)

780 pennate diatom (valve view), B) testate amoeba shell (*Euglypha cristata*), C) and D) sponge

781 spicules (fragments), E) elongate phytolith and F) bilobate phytolith. All scale bars: 50 µm.

782

783

784

785

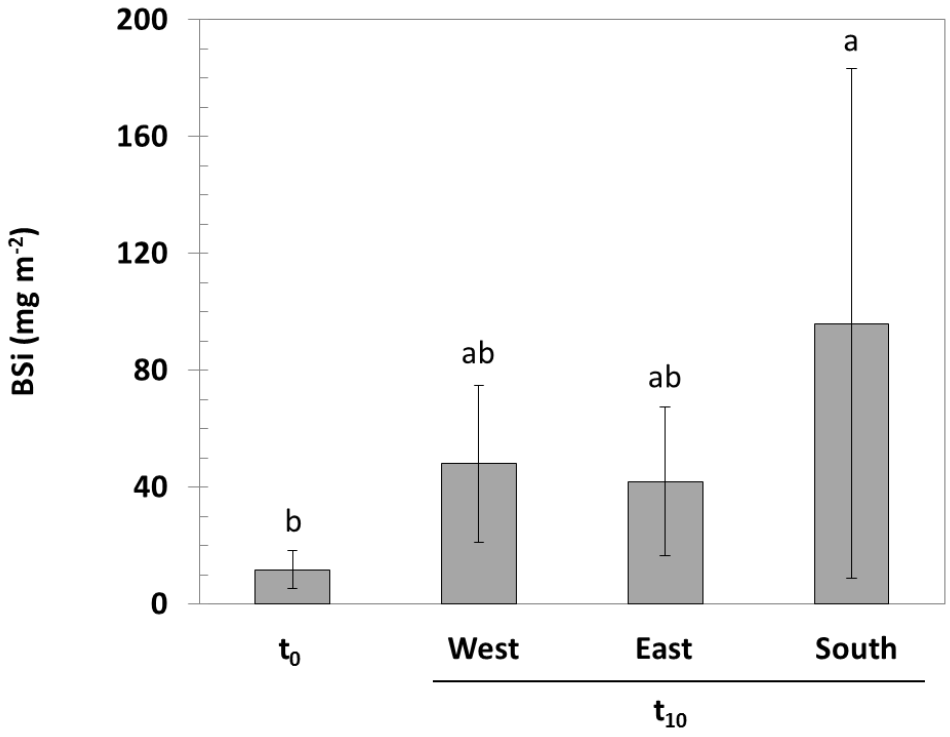


**Fig. 3.** Total biogenic Si pools in soils (means ± standard deviation, upper 5 cm) at Chicken Creek at the end of construction work ($t_0$) and after ten years of ecosystem development (western, eastern and southern sections, $t_{10}$). Significant differences are indicated by different letters ($p < 0.05$, Kruskal-Wallis ANOVA with Dunn's post hoc test).

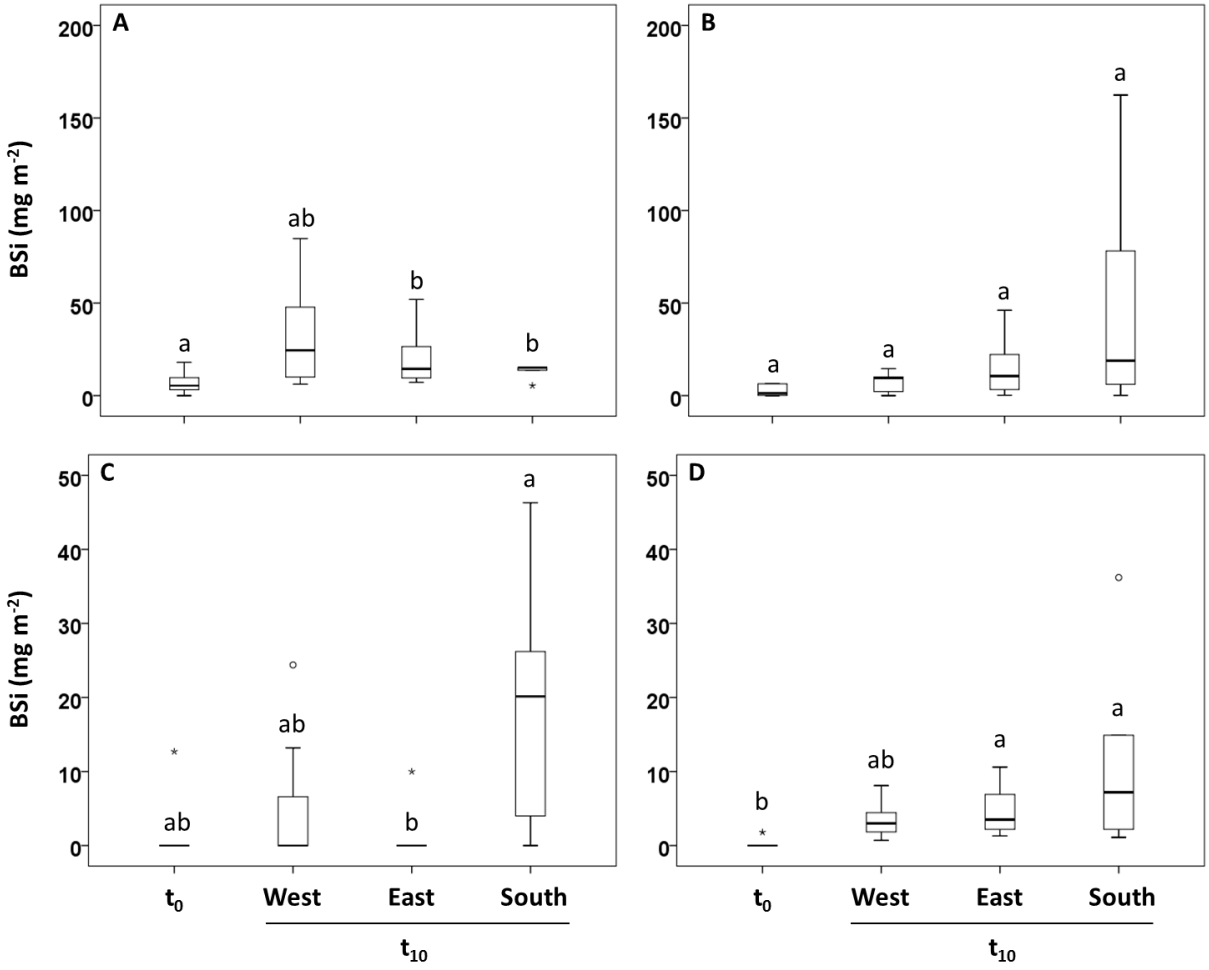


**Fig. 4.** Boxplots (top, middle and bottom lines of the boxes show the 25$^{th}$, 50$^{th}$ and 75$^{th}$ percentiles, respectively, and whiskers represent 1.5× the inter-quartile ranges) of biogenic Si pools in soils (upper 5 cm) at Chicken Creek at the end of construction work ($t_0$) and after ten years of ecosystem development (western, eastern and southern sections, $t_{10}$). A) Phytogenic Si pools (phytoliths), B) protophytic Si pools (diatom frustules), C) zoogenic Si pools (sponge spicules) and D) protozoic Si pools (testate amoeba shells). Significant differences are indicated by different letters ($p < 0.05$, Kruskal-Wallis ANOVA with Dunn's post hoc test). Circles and asterisks indicate outliers and extreme values, respectively. Note different scales for diagrams A+B and C+D.

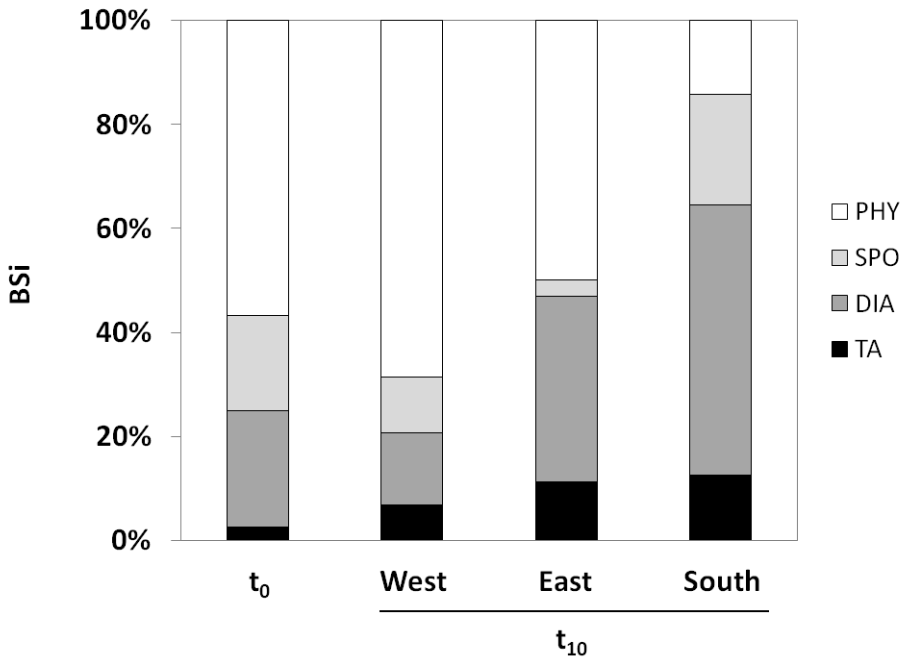


**Fig. 5.** Proportion of phytoliths (PHY), sponge spicules (SPO), diatom frustules (DIA) and testate amoeba shells (TA) to total BSi in soils (upper 5 cm) at Chicken Creek at $t_0$ and $t_{10}$. Note that total BSi pools differ in size (see Fig. 3).

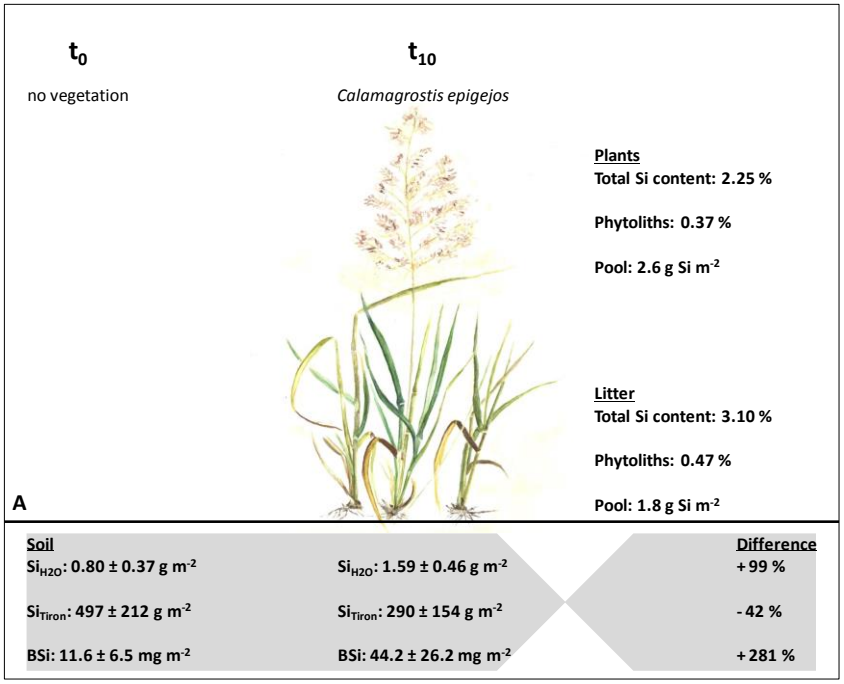


819

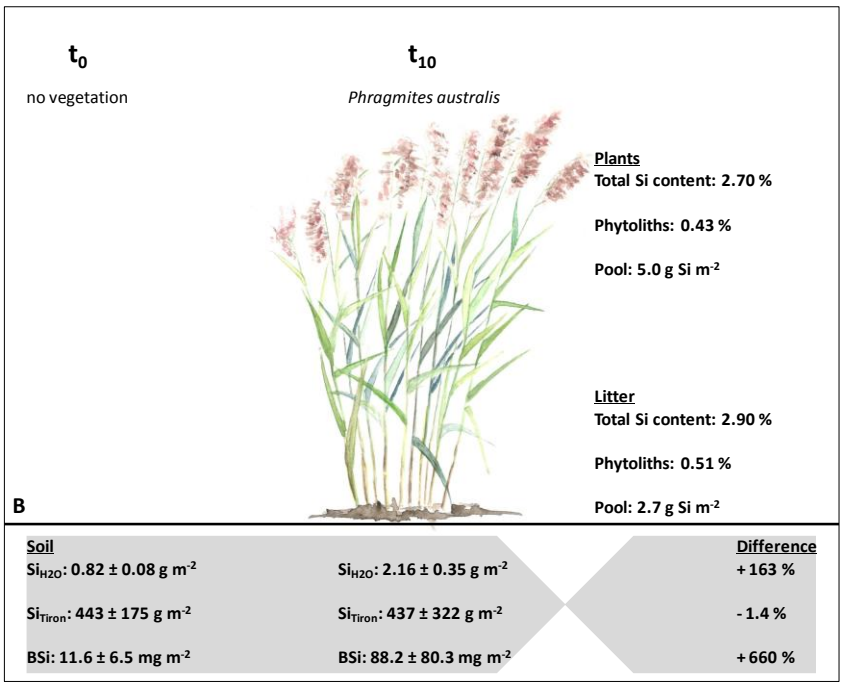


820

821 **Fig. 6.** Comparison of water soluble Si ($Si_{H2O}$) as well as amorphous Si ($Si_{Tiron}$) fractions and
822 total BSi in soils (means ± standard deviation, upper 5 cm), where *Calamagrostis epigejos* (A)
823 and *Phragmites australis* (B) became dominant. Data are given for $t_0$ (no vegetation) and $t_{10}$
824 (*C. epigejos*, *P. australis*). For $t_{10}$ total plant Si contents, extracted phytogenic Si (phytoliths)
825 contents and Si pools for *C. epigejos* and *P. australis* (plants and litter) are stated in addition.
826 Paintings from Cornelia Höhn, Müncheberg.

827 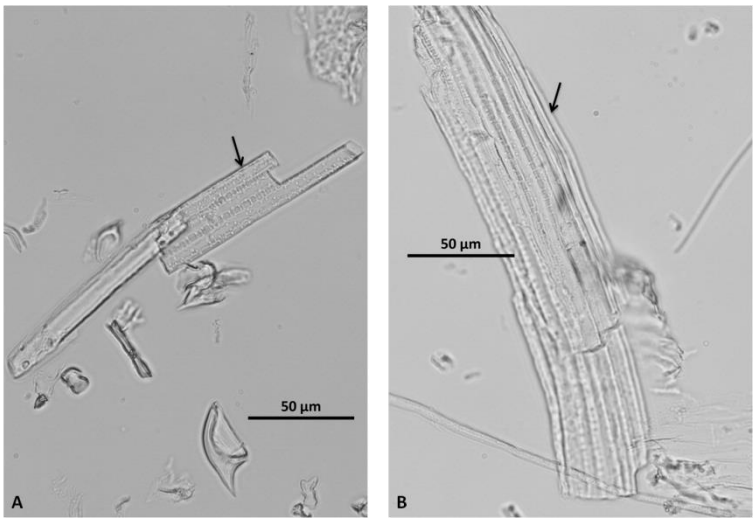


828 **Fig. 7.** Micrographs of fragile phytogenic Si structures (arrows) of *C. epigejos* (A) and *P.*
829 *australis* (B).

830

831

832

833

834

835

836

837

838

839

840

841

842

843

844

845 **Tables and Table headings**

846

847 **Table 1.** Contents of skeleton (>2 mm), fine earth (<2 mm), sand, silt and clay fractions
848 (upper 30 cm) at the sampling points in western, eastern and southern sections at Chicken
849 Creek ($t_0$, calculations based on data of Gerwin et al. 2010). Minimal (Min) as well as
850 maximal (Max) values, means ($\bar{x}$) and standard deviations (SD) are given.

| Section | | >2 mm | <2 mm | Sand | Silt | Clay |
|---|---|---|---|---|---|---|
| | | % | | | % | |
| West | Min | 9 | 80 | 77 | 7 | 5 |
| | Max | 20 | 91 | 88 | 13 | 10 |
| | $\bar{x}$ | 13 | 87 | 83 | 10 | 7 |
| | SD | 5 | 5 | 4 | 2 | 2 |
| East | Min | 2 | 77 | 69 | 6 | 4 |
| | Max | 23 | 98 | 91 | 20 | 11 |
| | $\bar{x}$ | 13 | 87 | 82 | 11 | 7 |
| | SD | 7 | 7 | 9 | 6 | 3 |
| South | Min | 0.2 | 84 | 78 | 7 | 4 |
| | Max | 17 | 99.8 | 89 | 17 | 8 |
| | $\bar{x}$ | 8 | 92 | 83 | 11 | 6 |
| | SD | 8 | 8 | 4 | 4 | 2 |

851

852

853

854

855

856

857

858

**Table 2.** Measured soil parameters (upper 5 cm, means ($\bar{x}$) with standard deviation (SD)) at the different sections of Chicken Creek. Significant differences between $t_0$ and $t_{10}$ are each stated in bold (Mann-Whitney U-test, p <0.05) or marked with asterisks (p <0.1) for the western, eastern and southern section.

| Age | Section | | $Si_{H2O}$ | $Si_{Tiron}$ | $Al_{Tiron}$ | $Fe_{Tiron}$ | $C_{org}$ | $CaCO_3$ | pH |
|---|---|---|---|---|---|---|---|---|---|
| | | | g $m^{-2}$ | | | | | | |
| $t_0$ | West | $\bar{x}$ | **0.70** | 524 | 312 | 249 | 237* | 88 | **7.9** |
| | | SD | 0.10 | 95 | 24 | 33 | 156 | 72 | 0.1 |
| $t_{10}$ | West | $\bar{x}$ | **1.73** | 552 | 254 | 239 | 556* | 101 | **7.4** |
| | | SD | 0.22 | 300 | 154 | 104 | 167 | 93 | 0.1 |
| $t_0$ | East | $\bar{x}$ | 0.87* | **503** | **268** | **261** | **123** | 91 | **8.1** |
| | | SD | 0.48 | 281 | 151 | 130 | 38 | 79 | 0.2 |
| $t_{10}$ | East | $\bar{x}$ | 1.50* | **196** | **122** | **151** | **396** | 30 | **7.1** |
| | | SD | 0.57 | 49 | 27 | 29 | 54 | 18 | 0.2 |
| $t_0$ | South | $\bar{x}$ | **0.84** | 399 | 232 | 238* | 160* | 174 | **8.3** |
| | | SD | 0.06 | 154 | 112 | 65 | 131 | 109 | 0.1 |
| $t_{10}$ | South | $\bar{x}$ | **2.24** | 317 | 147 | 157* | 474* | 126 | **7.4** |
| | | SD | 0.33 | 149 | 62 | 57 | 258 | 40 | 0.1 |

**Table 3.** Spearman's rank correlations between measured soil parameters and total BSi (upper 5 cm, n = 6) at Chicken Creek. Significant correlation coefficients are given in bold (p <0.05).

| | $Si_{H2O}$ | $Si_{Tiron}$ | $Al_{Tiron}$ | $Fe_{Tiron}$ | $C_{org}$ | $CaCO_3$ | pH | BSi |
|---|---|---|---|---|---|---|---|---|
| $Si_{H2O}$ | 1.000 | | | | | | | |
| $Si_{Tiron}$ | -0.257 | 1.000 | | | | | | |
| $Al_{Tiron}$ | -0.600 | **0.829** | 1.000 | | | | | |
| $Fe_{Tiron}$ | -0.486 | 0.771 | **0.943** | 1.000 | | | | |
| $C_{org}$ | 0.714 | 0.086 | -0.371 | -0.486 | 1.000 | | | |
| $CaCO_3$ | 0.200 | 0.086 | -0.086 | -0.029 | 0.029 | 1.000 | | |
| pH | -0.600 | 0.200 | 0.486 | 0.543 | -0.771 | 0.543 | 1.000 | |
| BSi | **0.941** | -0.213 | -0.577 | -0.577 | **0.880** | 0.152 | -0.698 | 1.000 |

870 **Table 4.** Surface-areas, volumes and surface-to-volume ratios (A/V) of different biogenic

871 siliceous structures found at Chicken Creek.

| | Surface-area (µm$^2$) | | Volume (µm$^3$) | | A/V ratio | |
|---|---|---|---|---|---|---|
| | **Min.** | **Max.** | **Min.** | **Max.** | **Range** | **Mean (SD)** |
| Bilobate phytoliths | 216 | 3,730 | 36 | 2,046 | 0.7-9.8 | 2.8 (1.8) |
| Elongate phytoliths | 2,302 | 22,203 | 390 | 14,649 | 0.6-5.9 | 2.6 (1.1) |
| Diatom frustules* | 351 | 9,901 | 347 | 28,024 | 0.3-3.3 | 0.9 (0.5) |
| TA shells* | 1,229 | 5,085 | 900 | 15,812 | 0.2-2.7 | 0.8 (0.7) |
| Sponge spicules* | 305 | 16,963 | 291 | 59,744 | 0.3-1.6 | 0.8 (0.4) |
| Spicule fragments* | 2,828 | 17,268 | 5,255 | 34,812 | 0.5-0.6 | 0.5 (0.03) |

872

873 * Data taken from Puppe et al. (2016).